Amphiphilic Block Copolymer Films: Phase Transition, Stabilization, and Nanoscale Templates

Jung Hyun Park,[†] Yujie Sun,[‡] Yale E. Goldman,[‡] and Russell J. Composto*,[†]

Department of Materials Science and Engineering and Nano/Bio Interface Center, University of Pennsylvania, Philadelphia, Pennsylvania 19104-6272, and Department of Physiology and Nano-Bio Interface Center, University of Pennsylvania, Philadelphia, Pennsylvania 19104-6083

Received October 17, 2008; Revised Manuscript Received December 12, 2008

ABSTRACT: A morphological transition of asymmetric poly(styrene-*b*-acrylic acid) (PS-*b*-PAA) films is observed by in situ scanning probe microscopy (SPM) in aqueous media. Upon initial exposure to buffer solution at pH 7.4, spherical PAA domains swell through a glassy PS surface layer to form negatively charged mushroom caps. With further exposure, the PAA caps coalesce to produce a smooth, highly wettable surface. However, if films are exposed to a buffer solution containing 3-aminopropyltriethoxysilane (APTES) for 1 h, the PAA domain swelling is greatly reduced and the mushroom caps stabilize at a diameter of 33 nm. This stabilization results from a cross-linking reaction between PAA and APTES, which also converts the PAA domains from a net negative to net positive charge. By varying molecular weights of PAA block in PS-*b*-PAA, the feature size and spacing can be tuned. To demonstrate an application for this template with positively charged domains, a cytoskeletal filament, F-Actin with a net negative charge, is organized on the PS-*b*-PAA template via electrostatic interactions under physiological conditions. F-Actin shows a tendency to align along the modified PAA mushroom caps.

Introduction

Designing soft materials for biological applications is of current interest.[1−8] For example, the adhesion of cells to hydrogels is greatest, and cell function optimized, when the compliance of the substrate matches that of the cell.[4,5] Researchers have also shown that endothelial cells can be aligned on micropatterned, elastomer substrates having parallel grooves and ridges made by soft lithography.[8] Depending on groove depth and width, cells and their cytoskeleton (i.e., filamentous Actin) orient parallel to grooves and the cells migrate faster along grooves than across. In addition to cells, biomolecules, such as proteins, have been patterned at the nanoscale using nanostructured material.[9−11] For example, biologically active antibodies, protein A/G, were covalently immobilized onto nanoscale arrays of 11-mercaptoundecanoyl-*N*-hydroxysuccinimide ester generated by dip-pen nanolithography.[9] Besides globular proteins, biopolymers such as DNA and filamentous Actin (F-Actin) have not been successfully patterned on nanostructured substrates under physiological conditions. At a larger length scale, Shin et al. have aligned λ-DNA along micropatterned aminopropyltriethoxysilane (APTES) by the electrostatic interaction between the phosphate backbone of DNA and amine groups on the surface.[12] In the present study, the goal is to align biopolymers on a soft nanostructured pattern under physiological conditions while preserving the native function of the molecule.

Block copolymers are one of the most successful examples of soft nanostructured materials that form by self-assembly.[13−15] Block copolymers are attractive templates for patterning biological molecules because they can form a range of structures by simply changing the volume fraction of each block.[16] In the bulk, self-assembled block copolymers that form spheres, cylinders, gyroids, and lamellae can be generated with a periodicity typically ranging from 10 to 100 nm.[16] For films, these structures can be further tuned by varying the surface and substrate properties as well as film thickness.[17−19] For example, immunoglobulin molecules are found to adsorb preferentially on parallel cylinders of poly(styrene) in a poly(styrene-*b*-methyl methacrylate) (PS-*b*-PMMA) film displaying a swirling, fingerprint pattern on the surface.[10] In another study, DNA molecules are found to stretch and align along perpendicular PMMA cylinders in a PS-*b*-PMMA film during drying process.[11] Whereas these studies are carried under ambient conditions, proteins should be imaged in a suitable aqueous media so that the functions and interactions of their native structures remain. In this respect, hydrophobic block copolymers are not particularly suitable as biomolecule templates in aqueous media. Therefore, a growing interest in amphiphilic block copolymers is emerging.[20−24]

Amphiphilic block copolymers (ABCs) are attractive as responsive materials because their swelling behavior can be tuned by ion concentration or pH.[22−24] For example, perpendicular cylinders of poly(acrylic acid) (PAA) surrounded by a poly(styrene) (PS) matrix are found to swell to form mushroom caps upon exposure of PS-*b*-PAA film to water at pH $\sim$ 5−6.[23] Swelling dynamics is explained by rapid diffusion of water into the domains followed by the slow relaxation of PAA chains. Upon varying pH, the extent of PAA swelling can be varied to create a series of unique surface morphologies.[24] Surface nanostructures are also fabricated in poly(styrene-*b*-2-vinylpyridine) (PS-*b*-P2VP) films by swelling the cylindrical P2VP phase, initially buried underneath the surface, with an acidic solution.[25,26] However, only nanostructured PS-*b*-PAA films are able to provide the selectivity for biological molecules to interact with hydrophilic or hydrophobic domains in physiological condition (pH $\sim$ 7). In addition, robustness of nanostructured templates is highly required for the in situ experiments of biological activities. Previous approaches to stabilize ABCs are to include glassy hydrophobic blocks that serve as physical cross-links.[20] Specifically, ABCs with two or more glassy hydrophobic blocks are needed to stabilize the microstructure upon swelling.

In this paper, we show that the microstructure of diblock copolymers can be retained by physically cross-linking the hydrophilic block. We investigate PS-*b*-PAA films containing

* Corresponding author: phone (215) 898-4451; fax (215) 573-2128; e-mail composto@seas.upenn.edu.
[†] Department of Materials Science and Engineering and Nano/Bio Interface Center.
[‡] Department of Physiology and Nano/Bio Interface Center.

10.1021/ma8023393 CCC: $40.75
Published on Web 01/16/2009

Scheme 1. (a) Chemical Transformation of PS-*b*-P*t*BA to PS-*b*-PAA by Thermal Deprotection of the *tert*-Butyl Groups Catalyzed by Surface Hydroxyl Groups; (b) Schematic Figure Showing How a Nanostructured Block Copolymer Template Is Created for F-Actin; (c) Idealization of the Chemical Reaction of PAA with APTES[a]

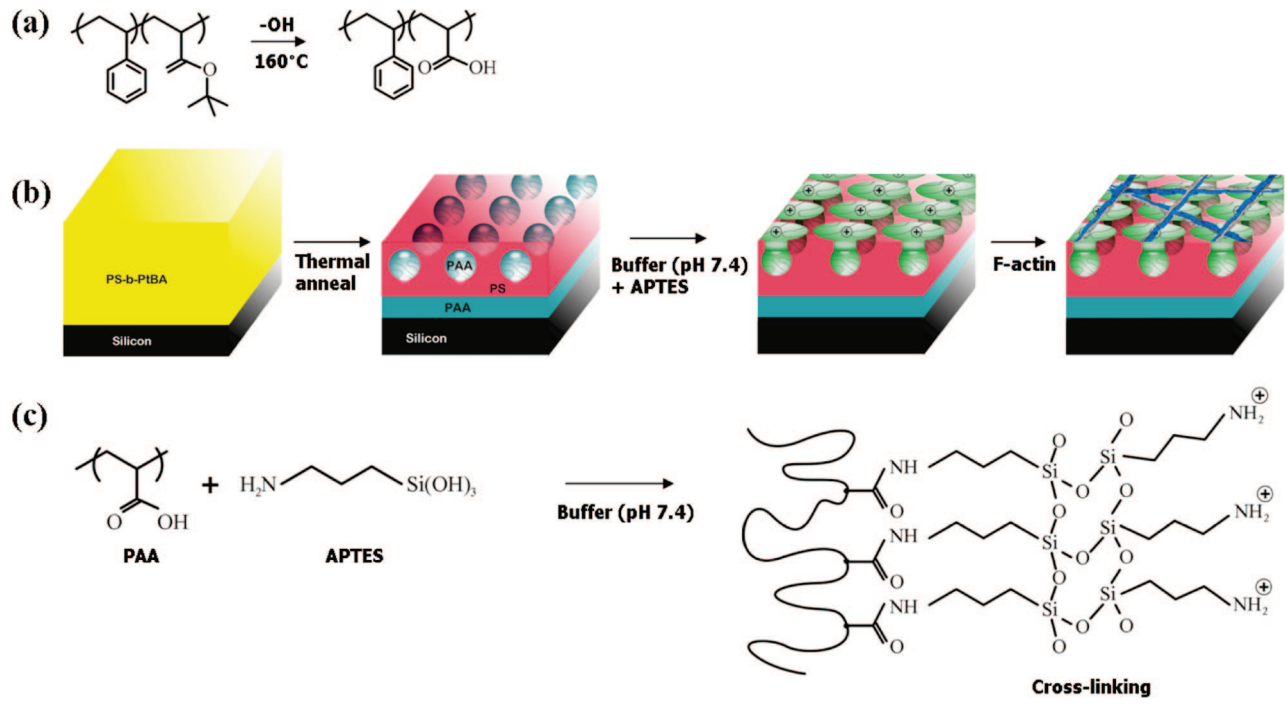

[a] The siloxane cross-links to inhibit the PAA domains from swelling to form a surface monolayer in buffer.[32] Unreacted amines produce positively charged domains.

PAA spheres that swell upon exposure to buffer solutions with pH 7.4. PAA domain growth is inhibited and stabilized if films are pretreated for 1 h with a buffer solution containing 3-aminopropyltriethoxysilane (APTES). This stabilized morphology of the PS-*b*-PAA film now displays positively charged features because of the incorporation of the amino groups from APTES into the PAA block. This template is then exposed to F-Actin under physiological conditions. Because of its negatively charged surface,[27,28] F-Actin is attracted to the modified PAA domains via electrostatic interaction. To the best of our knowledge, this approach to organize F-Actin has not been explored before.

Experimental Section

Film Preparation of PS-*b*-PAA. Poly(styrene-*b*-acrylic acid) (PS-*b*-PAA) is obtained by the thermal deprotection from poly(styrene-*b*-*tert*-butyl acrylate) (PS-*b*-P*t*BA).[29] PS-*b*-P*t*BA with molecular weights (*M*) of 66.2K−32K and 42K−8K are purchased from Polymer Source Inc. Because of weight loss during the chemical transformation of P*t*BA to PAA, the PAA block *M* is about 50% of P*t*BA *M*. The nomenclature and *M*'s are PS-*b*-PAA16K (66.2K−16K) and PS-*b*-PAA4K (42K−4K). Before film deposition, silicon wafers are treated with a piranha solution (98% H_2SO_4:30% H_2O_2 = 3:1) at 80 °C for 30 min followed by rinsing in water (Millipore Direct-Q, 18 MΩ·cm resistivity). After immersing in water for 1 day, substrates are dried by nitrogen gas. To remove organics and produce surface hydroxyl groups, substrates are exposed to UV-ozone (Model 42, Jelight Co. Inc.). Films are prepared by spin-casting from toluene solutions (1 wt % polymer). Block copolymer samples are annealed at 160 °C in Ar for 2 days. A buffer solution called M5 buffer (25 mM KCl, 20 mM Hepes (pH 7.6), 2 mM $MgCl_2$, 1 mM EGTA (Sigma, E4378)) is used for all experiments. To cross-link the PAA domains, APTES (0.5 vol %) is added to buffer solution.

Characterization. The surface functionality of films is characterized by contact angle measurements. After depositing a water droplet on the surface, the angle is determined using Scion Image software. The film thicknesses are measured with a Rudolf Research AutoEL-II Null ellipsometer. The film thicknesses decrease from its initial value, ∼40 nm, to ∼31 nm after the chemical transformation of P*t*BA to PAA. Refractive index values for pure PS and PAA are 1.59 and 1.53, respectively.[30] For PS-*b*-PAA, an average value of the pure components is used.

Scanning Probe Microscopy. Scanning probe microscopy (SPM, Agilent PicoPlus) is used to observe the surface morphology. For imaging in air and liquids, the acoustic ac mode and the magnetically driven ac mode are used, respectively. The spring constant (*k*) and tip radius of the magnetically coated cantilever or MAC Lever are 2.8 N/m and ∼7 nm, respectively. For F-Actin imaging, a softer tip called MACIV is used (k = 0.1 N/m). AFM images are analyzed by 2D fast Fourier transform (FFT) and grain analysis methods using SPIP software (Image Metrology, Inc.).

Preparation of F-Actin. F-Actin is polymerized from purified monomeric Actin (G-Actin). G-Actin is isolated and purified from rabbit muscle as described by Pardee and Spudich[31] and stored in G-Actin buffer (2 mM Tris buffer (pH 8.0), 0.2 mM $CaCl_2$, 0.2 mM ATP, and 0.5 mM DTT). To prepare 1.1 μM phalloidin (Molecular Probes, P3457) stabilized F-Actin, G-Actin is diluted to 1.33 μM with deionized H_2O and then mixed gently with deionized H_2O, 4× F-Actin buffer (300 mM KCl, 10 mM $MgCl_2$, 40 mM HEPES (pH 7.0), counts 1/4th of the final total volume), and 1.1 μM phalloidin (in that order). Then, the F-Actin solution is incubated at room temperature for 10 min, transferred onto ice, and stored at 4 °C with a shelf life up to 1 month. In order to obtain proper surface density of F-Actin, the F-Actin is diluted 3−5-fold in the M5 buffer.

Results and Discussion

An overview of the key results is given first followed by experimental details and analysis. In this paper, we demonstrate that PS-*b*-PAA films undergo a phase transformation due to the swelling of the PAA block upon exposure to buffer solution. A

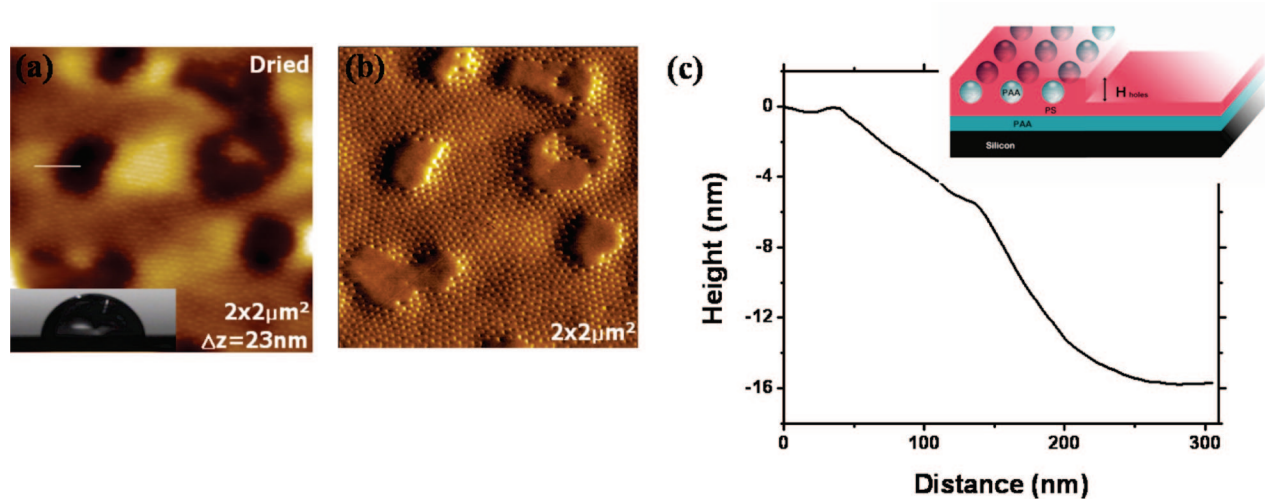

Figure 1. (a) SPM topography image and (b) phase image of PS-*b*-PAA16K annealed at 160 °C for 2 days in Ar. The contact angle of ∼90° in the inset suggests that a PS layer covers the surface. The phase image clearly captures the PAA spheres buried under the PS layer whereas the topography image shows small bumps ∼1 nm high. Because of the incommensurability of film thickness with the block copolymer period, large holes develop over the monolayer covering the substrate. The sphere diameter and block copolymer period are $D = 20 \pm 3.1$ nm and $L_0 = 42.9 \pm 2.6$ nm, respectively. (c) Height profile across the white line in (a) shows a hole depth of 16 nm. Schematic figure of the block copolymer morphology after annealing. The hole depth is indicated by H_{holes}.

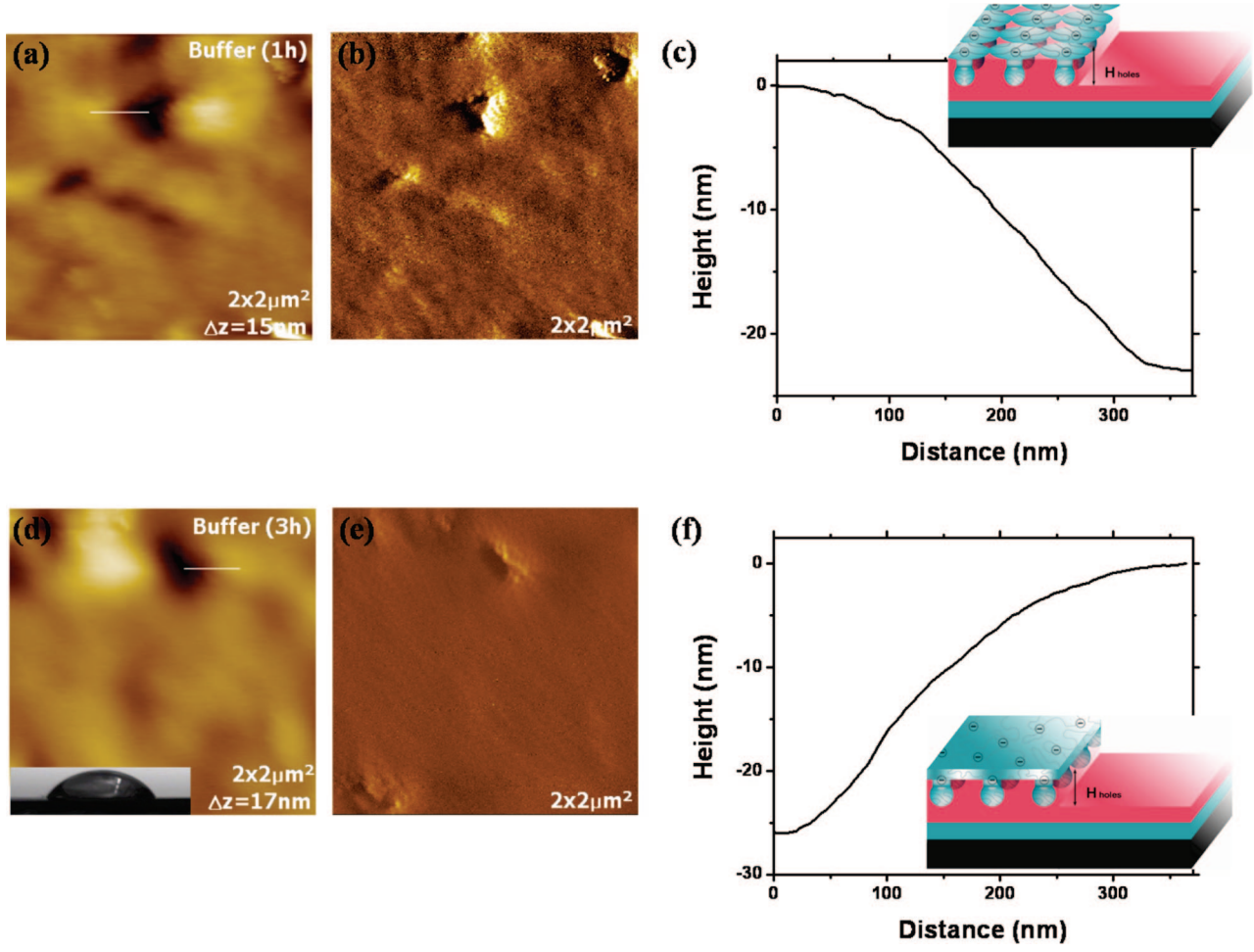

Figure 2. (a) In situ SPM topography image and (b) phase image of PS-*b*-PAA16K after 1 h exposure to buffer solution. (c) Height profile of a hole with an increased depth, ∼23 nm, with respect to the dried sample shown in Figure 1. Schematic figure showing the swollen mushrooms (inset). (d) Topography and (e) phase images after 3 h. (f) Height profile shows a hole depth of ∼26 nm. After 3 h, the mushroom caps have coalesced to form a smooth PAA monolayer as shown in the inset.

stabilized structure can be retained by cross-linking the PAA domains resulting in a nanoscale template for attaching biomolecules. A PS-*b*-P*t*BA film is chemically transformed into PS-*b*-PAA by thermal deprotection of the *tert*-butyl groups catalyzed by the hydroxyl (−OH) groups on the silicon oxide substrate at 160 °C, as shown in Scheme 1a. During conversion, the film thickness decreases from ∼40 to ∼31 nm due to *t*BA loss. Scheme 1b shows the processing steps including spin-

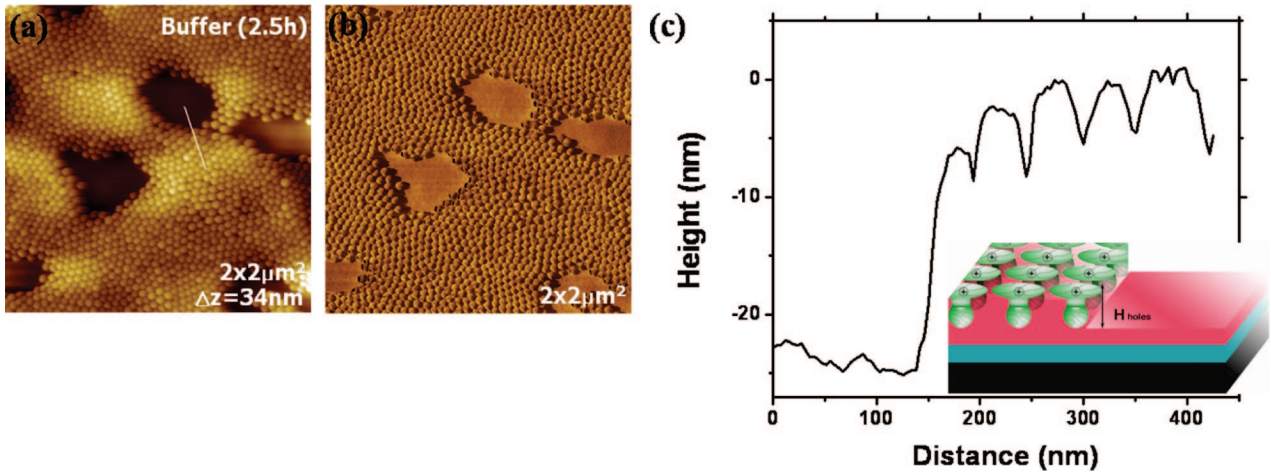

Figure 3. In situ SPM (a) topography and (b) phase images of PS-*b*-PAA16K stabilized by a buffer solution containing APTES. The images are taken after exposure to a neat buffer solution for 2.5 h. The discrete PAA domains are retained, and their diameter is 38.4 ± 5.4 nm, which is similar to the distance between domains, 43.9 ± 3.2 nm. The ratio of the diameter of PAA in dry and wet conditions is ~1.92. (c) The height profile taken across the white line in (a) shows periodic height variation due to the swollen PAA domains. Hole depth, ~22 nm, is measured between the top of the PAA domains and the bottom of the hole. The inset shows a stabilized morphology as well as the conversion of the negatively charged PAA (blue) to positively charged domains (green).

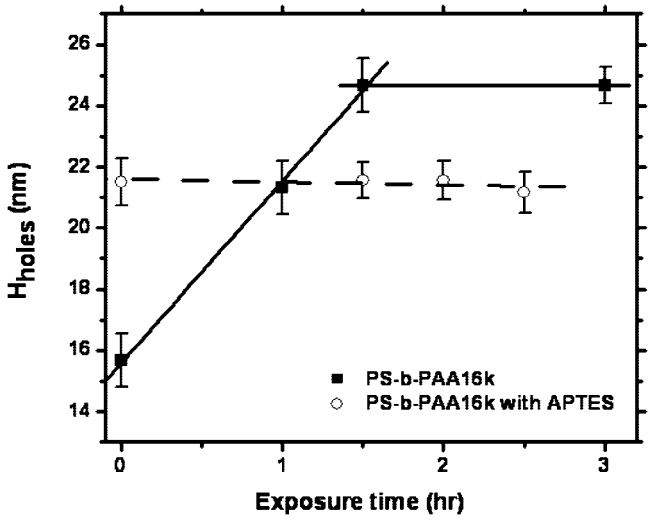

Figure 4. Hole depth of PS-*b*-PAA16K and APTES stabilized PS-*b*-PAA16K films as a function of exposure time to buffer solution. For the PS-*b*-PAA16K film, depth increases linearly and reaches an equilibrium value. However, for PS-*b*-PAA16K stabilized with APTES, the depth remains constant for up to 3 h exposure time.

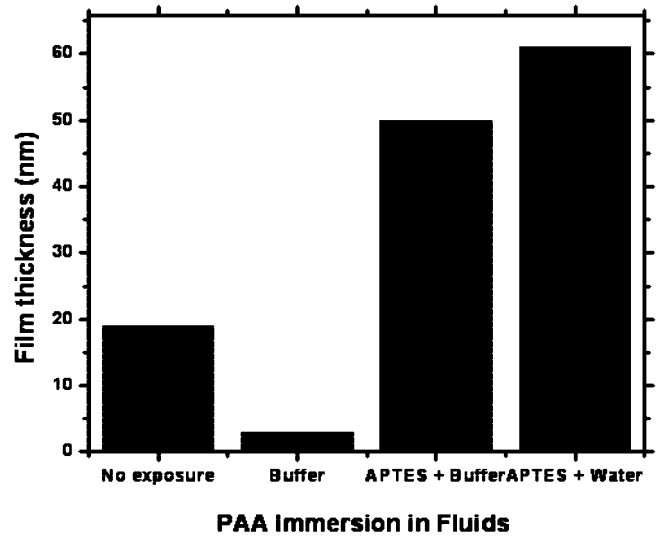

Figure 5. Film thickness of PAA homopolymer before and after exposure to aqueous solution. The original PAA film (~19 nm thick) nearly completely dissolves after exposure to the purely buffer solution. However, the one exposed to buffer containing APTES swells and gels to a thickness of 50 nm, 2.6 times the original thickness. The film exposed to Millipore water containing APTES swells by a factor of 3.2, consistent with lower cross-linking of PAA.

coating PS-*b*-P*t*BA (yellow), its conversion to PS-*b*-PAA, and the self-assembly of PAA domains. Because PS has a lower surface energy than PAA and PAA is preferentially attracted to the oxide, the initial or dry morphology consists of a buried, spherical array of PAA surrounded by a PS matrix. If this film is exposed to buffer solution at pH 7.4, the PAA spheres swell through the surface layer to form arrays of mushroom caps. However, if APTES is added to buffer solution, the PAA domains become cross-linked and their swelling is limited. A recent study has shown that APTES can attach to acceptor groups on the surface via the amine terminal group.[32] As shown in Scheme 1c, siloxane bond formation can occur between neighboring APTES molecules.[32] We attribute the reduced swelling of PAA domains to this cross-linking reaction. Moreover, this reaction allows for multilayer formation and, consequently, free amines within the PAA domains. The positively charged amines near the surface of the mushroom are likely responsible for the attraction of F-Actin on the template.

The surface morphology of PS-*b*-PAA16K films after annealing at 160 °C for 2 days in Ar is determined by SPM. Figure 1a,b shows an island/hole morphology with spherical arrays covering the high region and smooth lower regions. The PAA domains are discernible in the phase image (Figure 1b) because the underlying spheres perturb the modulus of the surface layer. The effective sphere diameter and period are 20 ± 3.1 and 42.9 ± 2.6 nm, respectively. As shown in the inset of Figure 1a, the water contact angle is ~90°, suggesting that the surface is entirely covered by PS. Thus, PAA spheres in the incomplete monolayer are initially protected by the PS shell; similarly, the PAA blocks adjacent to the substrate are covered by PS. Holes, about 0.5 μm in diameter, are observed in the top monolayer because the film thickness is incommensurate with the period, L_0, of PS-*b*-PAA. The height profile difference between the high and low regions gives the hole depth, H_{holes}, which is 16 nm, as shown in Figure 1c. Based on these SPM and contact angle results, the proposed morphology is shown in the inset of Figure 1c. Namely, the bottom layer consists of a lamellar-like region with the PAA block attracted to the oxide surface, whereas the

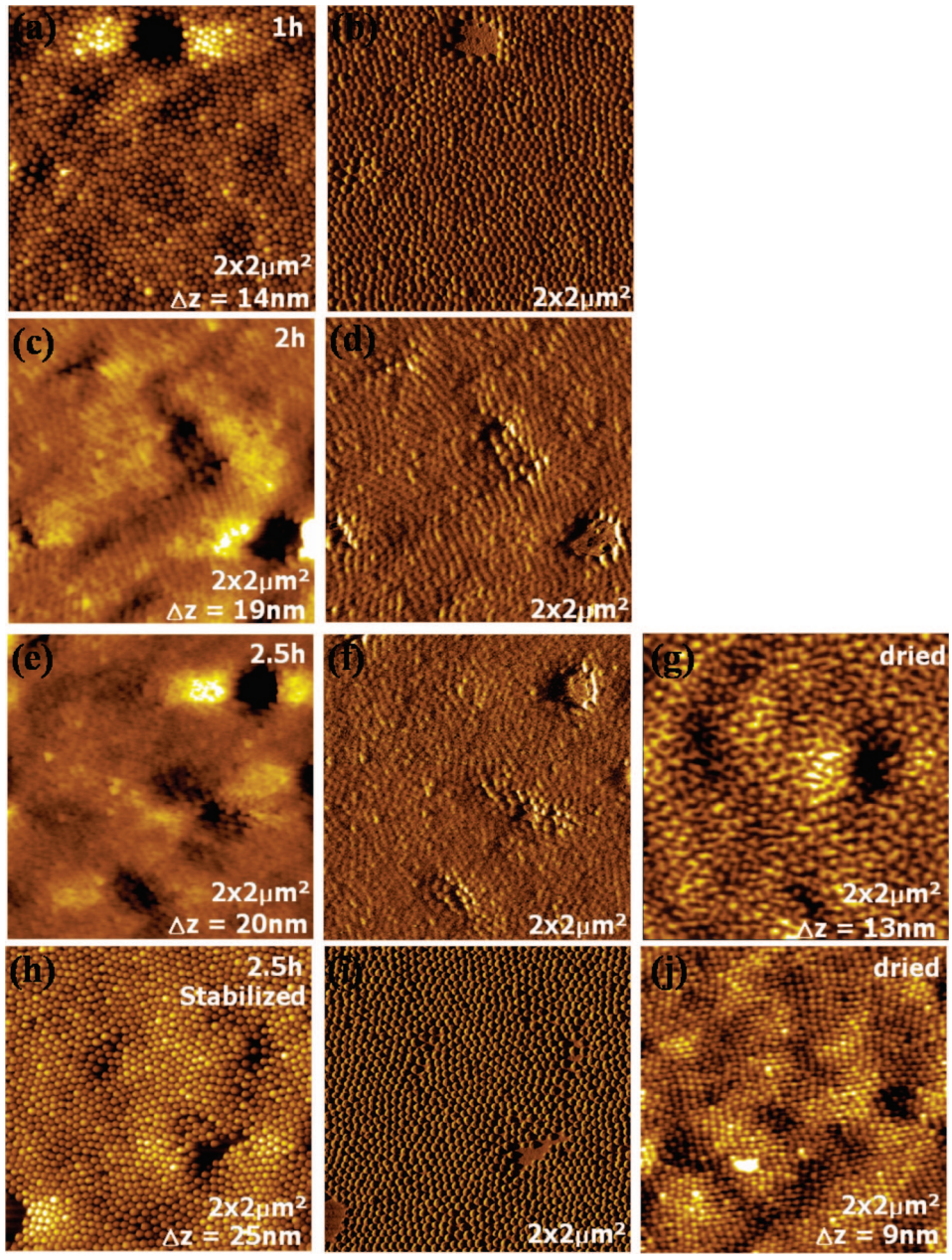

Figure 6. In situ SPM (a) topography and (b) phase images of PS-*b*-PAA4K after exposure to buffer solution for 1 h. Swollen PAA domains are shown. (c, d) After 2 h exposure, PAA domains begin to coalesce. (e, f) After 2.5 h exposure, PAA domains continue to coalesce. (g) After drying for 1 day, the PAA domains appear elongated. (h, i) After exposing to buffer containing APTES for 1 h, the PS-*b*-PAA4K film is immersed into buffer solution for 2.5 h. PAA domains swell but remain distinct. (j) After drying the stabilized PS-*b*-PAA4K film for 1 day, the topography image shows that PAA domains remain intact.

top layer is an incomplete monolayer of slightly compressed spheres.

After the PS-*b*-PAA16K film (Figure 1) is exposed to buffer solution at pH ∼ 7.4, the surface morphology evolves with immersion time as captured by the in situ SPM images in Figure 2. Because of the glassy PS matrix, the PAA spheres can only swell vertically to form mushroom-like caps. Parts a and b of Figure 2 show that the caps interpenetrate to form a smooth surface after 1 and 3 h, respectively. As shown in Figure 2c, H_{holes} increases to ∼23 nm, and fewer holes appear due to lateral swelling. The morphology after 1 h is shown in the inset of Figure 2c with the swollen PAA domains forming mushroom-like caps on the surface. After 3 h, Figure 2d,e shows the progressive swelling of the PAA domains, resulting in a featureless surface and an increase of H_{holes} to 26 nm, as shown in Figure 2f. After 3 h, the contact angle is ∼50° (inset of Figure 2d), suggesting that PAA, which has a contact angle of 42°, mainly covers the surface except in the few remaining holes (e.g., dark regions of Figure 2d). The reconstructed morphology is given in the inset of Figure 2f. Exposure of PS-*b*-PAA16K to buffer solution at pH 7.4 provides an interesting route to vary the surface energy from ∼90° (dry) to ∼50° (wet). However, for biological applications, controlled placement of molecules requires discrete features with controlled charge. Thus, we have developed a procedure that retains the PAA surface domains.

The morphological transition induced by swelling in buffer solution can be prevented by cross-linking the PAA domains. PAA is cross-linked by immersing films for 1 h in buffer solution (pH = 7.4) containing APTES. Cross-linked PS-*b*-PAA films are then exposed to the buffer solution for up to 2.5 h. Figure 3a,b shows the in situ morphology of the stabilized structure after 2.5 h. Similar to the dry state in Figure 1, the spherical domains are well-defined in the wet state and are stable for at least 2.5 h. The diameter is 38.4 ± 5.4 nm, which is

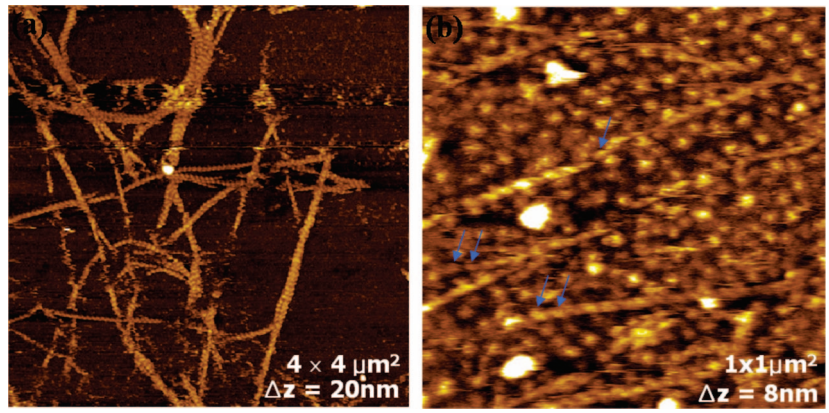

Figure 7. (a) In situ SPM topographic image of F-Actin on APTES-modified silicon. Individual filaments, bundles, and networks of F-Actin are observed. (b) In situ SPM topographic image of F-Actin on PS-*b*-PAA4K film stabilized by APTES. Negatively charged F-Actin is preferentially organized on the positively charged domains as indicated by the arrows. For both surfaces, F-Actin is adsorbed and imaged in identical conditions.

close to the distance between domains, 43.9 ± 3.2 nm. For comparison, the radius of gyration and contour length of the PAA block are 3 nm and 111 nm, respectively. Note that the diameter of the stabilized domains in the wet state is about twice that of the dry, namely, $D_{wet}/D_{dry} = 1.92$. Figure 3c shows that H_{holes} has increased from 16 nm (dry) to 22 nm in the wet state. Note that the spherical domains are easily distinguishable in the height profile. The resulting morphology is shown in the inset of Figure 3c.

H_{holes} in PS-*b*-PAA16K films is measured after exposure to a neat buffer solution as well as one containing APTES, as shown in Figure 4. In the buffer solution, the H_{holes} increases linearly until 1.5 h and then reaches an equilibrium value of ~25 nm. The hole growth velocity is 0.11 nm/min. These results differ from our previous study of PS-*b*-PAA swelling where the PAA domains are perpendicular cylinders. Upon exposure to water at pH 5−6, PAA caps grow rapidly as $t^{2.6}$ followed by a slower growth and finally a plateau region.[23] Because of the accelerated growth, equilibrium is reached after ~1 h faster than in the present study. This difference in growth behavior, in part, can be attributed to the direct exposure of PAA cylinders at the surface compared to PAA spheres buried under hydrophobic PS surface layer in the current study. Whereas H_{holes} increases by a factor of ~1.6 in buffer solution, the stabilized PS-*b*-PAA16K film maintains the same height, ~21.5 nm, for up to 3 h of exposure time, as shown in Figure 4. Note that this hole depth is about ~4 nm less than the value observed for the film prepared without APTES.

To further understand swelling of PS-*b*-PAA film, PAA films are deposited on silicon and exposed to various aqueous solutions. Figure 5 shows the thickness of the initial film (~19 nm) as well as the APTES stabilized film. After the PAA film is exposed to buffer solution, the thickness of the hydrophilic PAA film is only a few nanometers, consistent with dissolution of PAA. However, upon stabilizing with APTES, the PAA film swells in the buffer solution and reaches a thickness ~2.6 times the original value. As expected, this value is greater than the hole depth ratio, 1.4, between the stabilized and dried PS-*b*-PAA films given in Figure 4. Finally, when exposed to APTES dissolved in Millipore water (pH ~ 5−6), the film swells by a factor of 3.2. The increased swelling may be attributed to the lower pH which results in the reduced protonation of PAA and therefore fewer cross-links. To minimize swelling and retain PAA domains, APTES cross-linking of PAA in the film is carried out in buffer solution.

To further control domain size and separation, experiments are performed with PS-*b*-PAA4K, which has a PAA molecular weight that is 4 times less than PS-*b*-PAA16K. For the PS-*b*-PAA4K system, the distance between PAA domains, which are the attachment sites for F-Actin, is larger than in the PS-*b*-PAA16K system. This separation potentially allows for greater control over alignment of F-Actin. After exposure to buffer solution for 1 h, PAA domains appear as mushroom caps on the surface as shown in Figure 6a,b. In contrast to the PS-*b*-PAA16K film (Figure 2), PAA domains have not yet coalesced in the PS-*b*-PAA4K film after 1 h. After 2 h exposure, PAA domains have begun to coalesce and form a connected structure. After 2.5 h exposure, domains continue to coalesce but have not yet formed a smooth wetting layer on the surface. We attributed this behavior to a lower molecular weight of the PAA block which limits the extent of lateral stretching on the surface. For comparison, the PAA16K block is able to completely wet the surface, as shown in Figure 2d,e. Upon drying this film for 1 day, PAA domains shrink into irregularly shaped features that are well separated compared to the swollen film. To stabilize the PAA domain, PS-*b*-PAA4K film is exposed to buffer solution containing APTES for 1 h. After exposing this film to a buffer solution for 2.5 h, the PAA domains swell but remain as individual features because cross-linking prevents further expansion, as shown in Figure 6h,i. The diameter is 32.9 ± 4.2 nm, and the lateral periodicity is 44.3 ± 3.5 nm. Although the lateral periodicity is similar to the stabilized PS-*b*-PAA16K film, the PAA diameter is smaller. After drying for 1 day, the morphology is maintained as shown in Figure 6j. These results show that a decrease in the molecular weight of the PAA block leads to smaller domain size and more distinct features compared to the higher molecular weight system. Therefore, the PS-*b*-PAA4K system may be a better template for biomolecules attachment.

Finally, we demonstrate that the stabilized PS-*b*-PAA4K film can act as a template for attaching and organizing F-Actin. Previously, APTES monolayers have been used to attach DNA to substrates.[33] Similarly, F-Actin is attached to APTES-modified silicon under buffer solution. Figure 7a shows a SPM image of the negatively charged F-Actin immobilized on a positively charged APTES surface. This image is taken after 0.5 h in buffer solution, and similar ones are obtained up to 3 h. Successful attachment of F-Actin is also observed on a poly(dimethylaminoethyl methacrylate) (PDMAEMA) film. To demonstrate that a positively charged surface was needed to immobilize F-Actin, control experiments were performed by taking real-time total internal reflection fluorescence (TIRF) images of F-Actin on bare glass and unmodified PS-*b*-PAA films after 2 h immersion. For both surfaces, F-Actin is tethered to the substrate and fluctuates above the surface, indicating that APTES is necessary to induce immobilization of F-Actin on a

surface. Details are given in the Supporting Information. Figure 7a shows that the F-Actin forms bundles which assemble into a network structure. Individual F-Actin shows the helical structure with 36 nm pitch and a height of ~7 nm, in agreement with the reported value.[34−37] Lateral diameters in the image varied depending on the numbers of bundles. The measured width of F-Actin is ~20 nm, larger than expected because of SPM tip convolution.

In addition to stabilizing the morphology, APTES cross-linker converts PAA domains from negative to positive charge allowing for F-Actin attachment. At pH 7.4, the origin of positive charge is likely due to unreacted amines from APTES. Figure 7b shows that F-Actin is attached to PS-*b*-PAA4K film stabilized by APTES. The round features correspond to the modified PAA domains whereas long objects represent F-Actin. On the PS-*b*-PAA templates, F-Actin appears mainly as individual filaments, whereas on positively charged homogeneous surfaces, F-Actin mainly forms bundles and network structures. Studies are in progress to determine whether this difference in adsorption on patterned versus homogeneous surfaces is due to electrostatic and/or cation-mediated interactions. Presently, the short-range order of the PAA domains limits our ability to align F-Actin. In contrast to DNA, cytoskeleton molecules such as F-Actin and microtubules have long persistent lengths (>μm). Thus, present studies are underway to achieve long-range order of PAA domains using graphoepitaxy and zone refining.[38−41]

Conclusions

In conclusion, we have fabricated PS-*b*-PAA templates with controlled surface properties and feature sizes. Using in situ SPM imaging, PS-*b*-PAA16K and PS-*b*-PAA4K films are found to undergo a morphology transition upon exposure to buffer solution (pH ~ 7.4). Spherical PAA domains protrude through the PS surface layer and swell laterally across the surface. After 3 h, the surface morphology exhibits a smooth monolayer of PAA (PS-*b*-PAA16K) or partially interpenetrating PAA domains (PS-*b*-PAA4K). To limit swelling, PAA domains are cross-linked using APTES, which also converts these domains from negative to positive charge at pH 7.4. By tuning the molecular weights of PS-*b*-PAA, nanostructured templates having different feature sizes are prepared for the organization of biopolymers. F-Actin, a biopolymer with a negative surface charge, is immobilized on amine-containing surfaces including APTES and PS-*b*-PAA stabilized by APTES. On the template, F-Actin is attached and aligned with the domains via electrostatic interactions. These results demonstrate how biopolymers can be organized on self-assembled soft nanostructures. This approach can be extended to organize both flexible and rigid biopolymers such as DNA or microtubules.

Acknowledgment. This work is primarily supported by the Nano/Bio Interface Center at the University of Pennsylvania and the U.S. National Science Foundation under Grant DMR-0425780. Partial support is provided by NSF under Grants DMR-0549307 and DMR-0520020. We thank Professor Andrea J. Liu (PENN) for useful discussions, Dr. Craig Wall (Agilent) for advice regarding in situ liquid imaging of F-Actin, and Dr. Chen Xu (Arkema) for advice regarding the swelling behavior of ABCs.

Supporting Information Available: Real-time TIRF images of fluorescently labeled F-Actin were taken on bare glass and unmodified PS-*b*-PAA films after 2 h immersion in buffer solution. Prior to imaging, the substrates were incubated for 10 min and then washed with the buffer solution. The hydroxyl-rich glass surface and swollen PAA layer that covers the PS-*b*-PAA film partially repel the F-Actin. As a result, F-Actin molecules either attach by one end or fluctuate on the surface as shown in the accompanying movie. The size is 42 × 42 μm^2. This material is available free of charge via the Internet at http://pubs.acs.org.

References and Notes

(1) Chen, C. S.; Mrksich, M.; Huang, S.; Whitesides, G. M.; Ingber, D. E. *Science* **1997**, *276*, 1425–1428.
(2) Pelham, R. J.; Wang, Y. *Proc. Natl. Acad. Sci. U.S.A.* **1997**, *94*, 13661–13665.
(3) Levental, I.; Georges, P. C.; Janmey, P. A. *Soft Matter* **2007**, *3*, 299–306.
(4) Discher, D. E.; Janmey, P.; Wang, Y. *Science* **2005**, *310*, 1139–1143.
(5) Engler, A. J.; Richert, L.; Wong, J. Y.; Picart, C.; Discher, D. E. *Surf. Sci.* **2004**, *570*, 142–154.
(6) Engle, A.; Bacakova, L.; Newman, C.; Hategan, A.; Griffin, M.; Discher, D. *Biophys. J.* **2004**, *86*, 617–628.
(7) Solon, J.; Levental, I.; Sengupta, K.; Georges, P. C.; Janmey, P. A. *Biophys. J.* **2007**, *93*, 4453–4461.
(8) Uttayarat, P.; Toworfe, G. K.; Dietrich, F.; Lelkes, P. I.; Composto, R. J. *J. Biomed. Mater. Res., Part A* **2005**, *75A*, 668–680.
(9) Lee, S. W.; Oh, B.; Sanedrin, R. G.; Salaita, K.; Fujigaya, T.; Mirkin, C. A. *Adv. Mater.* **2006**, *18*, 1133–1136.
(10) Kumar, N.; Hahm, J. *Langmuir* **2005**, *21*, 6652–6655.
(11) Liu, G.; Zhao, J. *Langmuir* **2006**, *22*, 2923–2926.
(12) Shin, M.; Kwon, C.; Kim, S. K.; Kim, H. J.; Roh, Y.; Hong, B.; Park, J. B.; Lee, H. *Nano Lett.* **2006**, *6*, 1334–1338.
(13) Park, M.; Harrison, C.; Chaikin, P. M.; Register, R. A.; Adamson, D. H. *Science* **1997**, *276*, 1401–1404.
(14) Thurn-Albrecht, T.; Schotter, J.; Kastle, G. A.; Emley, N.; Shibauch, T.; Krusin-Elbaum, L.; Guarini, K.; Black, C. T.; Tuominen, M. T.; Russell, T. P. *Science* **2000**, *290*, 2126–2129.
(15) Hadziioannou, G. *MRS Bull.* **2002**, 456–460.
(16) Bates, F. S. *MRS Bull.* **2005**, *30*, 525–532.
(17) Russell, T. P.; Menelle, A.; Anastasiadis, S. H.; Satija, S. K.; Majkrzak, C. F. *Macromolecules* **1991**, *24*, 6263–6269.
(18) Fasolka, M. J.; Banerjee, P.; Mayes, A. M. *Macromolecules* **2000**, *33*, 5702–5712.
(19) Chen, D.; Gong, Y.; Huang, H.; He, T. *Macromolecules* **2007**, *40*, 6631–6637.
(20) Topham, P. D.; Howse, J. R.; Mykhaylyk, O. O.; Armes, S. P.; Jones, R. A. L.; Ryan, A. J. *Macromolecules* **2006**, *39*, 5573–5576.
(21) Wang, C.; Mao, Y.; Wang, D.; Qu, Q.; Yang, G.; Hu, X. *J. Mater. Chem.* **2008**, *18*, 683–690.
(22) Currie, E. P. K.; Sieval, A. B.; Fleer, G. J.; Cohen Stuart, M. A. *Langmuir* **2000**, *16*, 8324–8333.
(23) Xu, C.; Fu, X.; Fryd, M.; Xu, S.; Wayland, B. B.; Winey, K. I.; Composto, R. J. *Nano Lett.* **2006**, *6*, 282–287.
(24) Xu, C.; Wayland, B. B.; Fryd, M.; Winey, K. I.; Composto, R. J. *Macromolecules* **2006**, *39*, 6063–6070.
(25) Chai, J.; Wang, D.; Fan, X.; Buriak, J. M. *Nat. Nanotechnol.* **2007**, *2*, 500–506.
(26) Chai, J.; Buriak, J. M. *ACS Nano* **2008**, *2*, 489–501.
(27) Tang, J. X.; Janmey, P. A. *J. Biol. Chem.* **1996**, *271*, 8556–8563.
(28) Tuszynski, J. A.; Portet, S.; Dixon, J. M.; Luxford, C.; Cantiello, H. F. *Biophys. J.* **2004**, *86*, 1890–1903.
(29) La, Y.; Edwards, E. W.; Park, S.; Nealey, P. F. *Nano Lett.* **2005**, *5*, 1379–1384.
(30) Brandrup, J.; Immergut, E. H.; Crulke, E. A. *Polymer Handbook*, 4th ed.; John Wiley & Sons: New York, 1999.
(31) Pardee, J. D.; Spudich, J. A. *Methods Cell Biol.* **1982**, *24*, 271–289.
(32) Howarter, J. A.; Youngblood, J. P. *Macromolecules* **2007**, *40*, 1128–1132.
(33) Liu, Z.; Li, Z.; Zhou, H.; Wei, G.; Song, Y.; Wang, L. *J. Microsc.* **2005**, *218*, 233–239.
(34) Holmes, K. C.; Popp, D.; Gebhard, W.; Kabsch, W. *Nature (London)* **1990**, *347*, 44–49.
(35) Tang, J. X.; Janmey, P. A. *Biol. Bull.* **1998**, *194*, 406–408.
(36) Shao, Z.; Shi, D.; Somlyo, A. V. *Biophys. J.* **2000**, *78*, 950–958.
(37) Shi, D.; Somlyo, A. V.; Somlyo, A. P.; Shao, Z. *J. Microsc.* **2001**, *201*, 377–382.
(38) Segalman, R. A.; Yokoyama, H.; Kramer, E. J. *Adv. Mater.* **2001**, *13*, 1152–1155.
(39) Sundrani, D.; Darling, S. B.; Sibener, S. J. *Nano Lett.* **2004**, *4*, 273–276.
(40) Cheng, J. Y.; Ross, C. A.; Thomas, E. L.; Smith, H. I.; Vancso, G. J. *Appl. Phys. Lett.* **2002**, *81*, 3657–3659.
(41) Berry, B. C.; Bosse, A. W.; Douglas, J. F.; Jones, R. L.; Karim, A. *Nano Lett.* **2007**, *7*, 2789–2794.

MA8023393